Theory of Magnetodynamics Induced by Spin Torque in Perpendicularly Magnetized Thin Films

M. A. Hoefer,[1,*] M. J. Ablowitz,[1] B. Ilan,[1] M. R. Pufall,[2] and T. J. Silva[2]

[1]*Department of Applied Mathematics, University of Colorado, Boulder, Colorado 80309-0526, USA*
[2]*National Institute of Standards and Technology, Boulder, Colorado 80305, USA*
(Received 30 June 2005; published 23 December 2005)

A nonlinear model of spin-wave excitation using a point contact in a thin ferromagnetic film is introduced. Large-amplitude magnetic solitary waves are computed, which help explain recent spin-torque experiments. Numerical simulations of the fully nonlinear model predict excitation frequencies in excess of 0.2 THz for contact diameters smaller than 6 nm. Simulations also predict a saturation and redshift of the frequency at currents large enough to invert the magnetization under the point contact. The theory is approximated by a cubic complex Ginzburg-Landau type equation. The mode's nonlinear frequency shift is found by use of perturbation techniques, whose results agree with those of direct numerical simulations.

Microwave generation due to spin-momentum transfer (SMT) in a thin magnetic multilayer is of current interest with potential applications in communications. Initial predictions based upon a linear theory [1] were recently verified experimentally [2–4]. In Refs. [2,4], microwaves were generated by the application of a dc current through a nanocontact to a magnetic multilayer (see Fig. 1). Recent nonlinear theories have neglected spatial variation [5]. In this study, a nonlinear theory of *spatially nonuniform* magnetodynamics is developed and analyzed.

The system depicted in Fig. 1 has been shown experimentally to give rise to microwaves caused by steady-state precession of magnetization in the ferromagnetic free layer ($Ni_{80}Fe_{20}$) [4]. A magnetic field $\vec{H}_0$ is applied perpendicular to the film plane. When a dc current, I, is applied through a point contact into the multilayer $Co_{90}Fe_{10}/Cu/Ni_{80}Fe_{20}$, the conduction electrons' spins induce a torque on the magnetization in the free layer due to conservation of angular momentum [1,6]. This torque opposes the damping of the free layer and produces dynamics. Slonczewski's linear theory of spin-wave excitation for point contacts on magnetic multilayers predicts a threshold current for the excitation of precession [7]. However, it does not accurately predict the experimentally observed frequencies nor the dependence of the frequency on current.

Understanding the SMT effect in point contacts with a perpendicular geometry is of great interest as it yields the narrowest linewidths and highest output powers [4,8] when compared to other SMT geometries, such as nanopillars [3] and in-plane fields [9]. In addition, this highly symmetric configuration is most amenable to analytical study. Insights derived from this simpler geometry may aid in solving the more advanced problem of oblique angled fields.

In this Letter we derive a new complex cubic Ginzburg-Landau (CGL) equation for weakly nonlinear excitations. Dipole coupling and exchange nonlinearities result in frequencies higher than Slonczewski's predictions. Steady-state precessing modes for a nonlinear vectorial model are found via numerical integration. The calculated frequen-

cies lie in the range of experimental observations [4]. Using this model, much higher frequencies (0.2 THz) are predicted for systems with contact radii on the order of $r_* = 3$ nm. The saturation and redshift of frequency for currents large enough to invert the magnetization under the point contact are predicted. This is a direct consequence of the exchange term included in our model.

Zero temperature dynamics of the free layer magnetization $\vec{M}$ can be described by the vectorial equation

$$\frac{\partial \vec{M}}{\partial \tau} = \underbrace{-|\gamma|\mu_0 \vec{M} \times \vec{H}_{\text{eff}}}_{\text{precession}} - \underbrace{\frac{2}{M_s^2 T_2}\vec{M} \times (\vec{M} \times \vec{H}_{\text{eff}})}_{\text{Landau-Lifshitz damping}}$$
$$+ \underbrace{\beta(\vec{x})\vec{M} \times (\vec{M} \times \hat{m}_{\text{F}})}_{\text{Slonczewski SMT torque}}, \qquad (1)$$

where the precessional and damping terms are driven by the effective magnetic field $\vec{H}_{\text{eff}} = H_0\hat{z} - M_z\hat{z} + \frac{2\pi D}{\gamma\mu_0 M_s h}\nabla^2\vec{M}$. This field consists of the applied magnetic field, the demagnetizing field due to axial dipole coupling, and the exchange field [10]. Crystalline anisotropy is as-
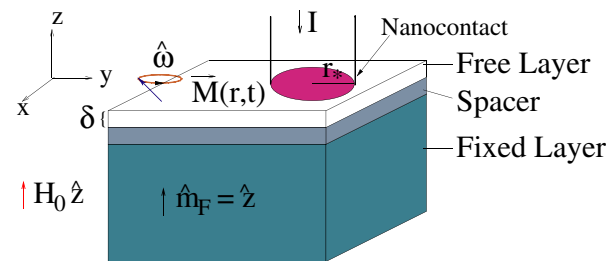

FIG. 1 (color online). Magnetic multilayer with magnetization $\vec{M}$ precessing in the free layer with frequency $\hat{\omega}$. The magnetization of the lower ferromagnetic layer is fixed with orientation $\hat{m}_F$. A nonmagnetic spacer is sandwiched between two ferromagnetic layers. Typical parameters are: $r_* = 20$ nm and $\delta = 5$ nm.

sumed to be negligible. The Landau-Lifshitz form of
damping is a commonly used phenomenological term
that drives the magnetization to align with the total field.
The Slonczewski SMT torque term is derived in [1] and
assumes a large, bulk ferromagnetic layer with fixed mag-
netization direction $\hat{z}$. The SMT torque term is derived
from semiclassical considerations and conserves angular
momentum. As such, inclusion of such a term into the
Landau-Lifshitz equation is helpful for gaining insight
into the coarse-grained dynamics of the system. Relevant
parameters are the gyromagnetic ratio (γ), Planck's con-
stant (h), the free space permeability (μ_0), the exchange
parameter (D), the saturation magnetization (M_s), and the
transverse relaxation time (T_2); $\beta(\vec{x})$ is the SMT driving
term.

The magnetization is assumed to have rotational sym-
metry: the spatial variation of the magnetization depends
solely on the distance r from the center of the point contact.
Then, the driving term, β, is given by

$$\beta(r) = \frac{I\hbar\epsilon\gamma}{2M_s^2\delta\pi r_*^2 e}\Phi(r_* - r),$$

$$\Phi(r_* - r) = \begin{cases} 1 & r \le r_* \\ 0 & r > r_* \end{cases},$$

where ϵ is the SMT efficiency, δ is the thickness of the free
layer, e is the charge of an electron, $r = (x^2 + y^2)^{1/2}$, and
$\Phi(r_* - r)$ is the Heaviside step function defining the point
contact to be a circle of radius r_*. The efficiency ϵ is in
principle a complicated function of many parameters, in-
cluding (but not limited to) microscopic details of the
interfaces in question [7,11]. Many of the approximations
used in the calculation of ϵ ignore the lateral geometry of
the actual experiments, choosing instead to use a more
tractable 1D calculation. Since ϵ is difficult to approxi-
mate, let alone calculate, and is not the subject of this
Letter, we will treat ϵ as a constant fitting parameter.

By taking the dot product of Eq. (1) with $\vec{M}$, one sees
that the magnetization of the free layer is locally conserved
for all times, i.e., $|\vec{M}| = M_s$. Consider the standard nor-
malization, $\vec{m} = \vec{M}/M_s = (m_x, m_y, m_z)$, $t = \omega_M \tau$, $\rho = r/l_{ex}$, where $\omega_M \equiv \gamma\mu_0 M_s$ and the exchange length is
$l_{ex} \equiv \sqrt{2\pi D/\gamma\mu_0 M_s h}$. For the analysis, it is convenient
to encode the transverse components of $\vec{m}$, $\vec{m}_\perp = (m_x, m_y)$,
in the complex quantity $m = m_x + im_y$. Evaluating the
vector cross products in (1) leads to

$$i\frac{\partial m}{\partial t} = -m\nabla^2 m_z + (m_z + i\alpha)\nabla^2 m + (m_z - h)m$$
$$+ i\{j\Phi(\rho_* - \rho) - \alpha(h - m_z)\}m_z m + i\alpha\{|\nabla m_z|^2$$
$$+ |\nabla m|^2\}m \qquad (2)$$

$$\frac{\partial m_z}{\partial t} = -\text{Im}(m^*\nabla^2 m) + \{\alpha(h - m_z) - j\Phi(\rho_* - \rho)\}|m|^2$$
$$+ \alpha\{\nabla^2 m_z + (|\nabla m|^2 + |\nabla m_z|^2)m_z\}.$$

The dimensionless parameters for applied field, damping,
and current are, respectively,

$$h = \frac{H_0}{M_s}, \qquad \alpha = \frac{2}{\gamma\mu_0 M_s T_2}, \qquad j = \frac{\hbar\epsilon}{2M_s^2 e\mu_0\pi r_*^2\delta}I.$$

The coupled system (2) is equivalent to the model (1).
Since the patterned multilayer mesa used in experiments
is 2 orders of magnitude wider than the point contact [4],
we assume that the multilayer has infinite extent in the xy
plane, hence $0 \le \rho < \infty$.

The *nominal* parameter values used in this Letter are
$r_* = 20$ nm, $\epsilon = 0.26$, $D = 4$ meV $\cdot$ nm^2, $M_s = 640$ kA/m, $\delta = 5$ nm, $\gamma = 1.85 \times 10^{11}$ Hz/T, $\omega_M = 23.68$ GHz, $l_{ex} = 6.40$ nm, and $\alpha = 0.0112$. We show
that by using only ϵ as a fitting parameter, the theoretical
data match experiment well. Except where noted, the
parameter values $h = 1.1$ and $\rho_* = 3.12$ are used.

In order to develop a perturbation scheme, we introduce
a small parameter, $\frac{a^2}{2} \ll 1$, and a rescaling of Eq. (2), $m = a\tilde{m}$. The parameter a represents the magnitude scale of the
transverse magnetization at the center of the point contact.
Using the approximation, $m_z \approx 1 - \frac{a^2}{2}|\tilde{m}|^2$ for the satura-
tion condition, substituting this approximation into Eq. (2),
and keeping only first-order terms in a^2, we find that $\tilde{m}$
satisfies a CGL-type equation,

$$i\frac{\partial\tilde{m}}{\partial t} = (1 + i\alpha)\nabla^2\tilde{m} - (h - 1)\tilde{m} + i\{j\Phi - \alpha(h-1)\}\tilde{m}$$

$$+ \frac{a^2}{2}\{\underbrace{-|\tilde{m}|^2\tilde{m}}_{\text{dipole coupling}} + i[j\Phi - \alpha(h-2)]|\tilde{m}|^2\tilde{m}$$

$$+ \underbrace{[\tilde{m}\nabla^2\tilde{m}^* + 2(1 + i\alpha)|\nabla\tilde{m}|^2]\tilde{m}}_{\text{nonlinear exchange}}\}. \qquad (3)$$

Seeking a steady-state solution of the form $\tilde{m}(\rho, t) = e^{i\hat{\omega}t}\phi(\rho)$, $\hat{\omega} = h - 1 - \omega$ yields a *nonlinear* eigenvalue
problem with boundary conditions $\phi(0) = 1$, $d\phi/d\rho(0) = 0$, $\lim_{\rho\to\infty}\phi(\rho) = 0$. The corresponding *linear* eigenvalue
problem was solved by Slonczewski [7] with two real
eigenvalues ω and j and bessel type eigenfunctions. This
suggests the asymptotic expansions

$$\phi(\rho) = \phi^{(0)}(\rho) + \frac{a^2}{2}\phi^{(1)}(\rho) + \cdots$$

$$\omega = \omega^{(0)} + \frac{a^2}{2}\omega^{(1)} + \cdots, \qquad j = j^{(0)} + \frac{a^2}{2}j^{(1)} + \cdots. \qquad (4)$$

The terms $\phi^{(0)}$, $\omega^{(0)}$, and $j^{(0)}$ correspond to Slonczewski's
linear solution.

The predicted frequency of the ground state mode, $\hat{\omega} \sim h - 1 - \omega^{(0)}$, is valid only for very small amplitudes a,
whereas experiments produce much higher frequencies [4].
The nonlinearity in (3) gives rise to a frequency shift
which, through the use of the Poincaré method [12], helps
explain this disparity.

Nonlinear solution:—The first-order nonlinear frequency and critical current shifts $\omega^{(1)}$ and $j^{(1)}$ are determined by the linear system

$$\begin{bmatrix} \mathrm{Re}\,(I_2) & \mathrm{Im}\,(I_1) \\ \mathrm{Im}\,(I_2) & -\mathrm{Re}\,(I_1) \end{bmatrix} \begin{bmatrix} \omega^{(1)} \\ j^{(1)} \end{bmatrix} = \begin{bmatrix} \mathrm{Re}\,(I_3) + \mathrm{Im}\,(I_4) \\ \mathrm{Im}\,(I_3) - \mathrm{Re}\,(I_4) \end{bmatrix},$$

where I_k depend only on the leading-order solution:

$$I_1 \equiv \frac{\rho_*^2}{2} \{ J_0^2(k_i \rho_*) + J_1^2(k_i \rho_*) \}$$

$$I_2 \equiv I_1 - \frac{c^2 \rho_*^2}{2} \{ [H_0^{(2)}(k_o \rho_*)]^2 + [H_1^{(2)}(k_o \rho_*)]^2 \}$$

$$I_3 \equiv \int_0^\infty \{ -|\phi^{(0)}|^2 + \phi^{(0)} \nabla^2 \phi^{(0)*} + 2|\nabla\phi^{(0)}|^2 \} \phi^{(0)2} \rho \, d\rho$$

$$I_4 \equiv \int_0^\infty \{ \alpha(2-h)|\phi^{(0)}|^2 - 2\alpha|\nabla\phi^{(0)}|^2 \} \phi^{(0)2} \rho \, d\rho$$
$$+ j^{(0)} \int_0^{\rho_*} |\phi^{(0)}|^2 \phi^{(0)2} \rho \, d\rho.$$

The above perturbation method provides a means for calculating the nonlinear frequency and current shifts, $\omega^{(1)}$ and $j^{(1)}$, of a mode solution to (3) and helps explain experimental results [2]. The frequency and critical current have a parabolic dependence on the transverse amplitude a

$$\hat{\omega} \sim h - 1 - \omega^{(0)} - \frac{a^2}{2}\omega^{(1)}, \qquad j \sim j^{(0)} + \frac{a^2}{2} j^{(1)}. \quad (5)$$

We note that using Eqs. (5), the relation between $\hat{\omega}$ and j is linear because both scale as a^2.

The first-order nonlinear contributions from Eq. (3) due to exchange and dipole coupling were compared. Using Eqs. (5), the frequency and current dependence as parametrized by a were calculated when the exchange and dipole coupling nonlinearities were removed from the calculation. We find that if nonlinear exchange terms are ignored, the relative error in the slope $d\hat{\omega}/dj$ is approximately 10% for $r_* = 20$ nm, whereas for $r_* < 12$ nm the relative error is greater than 25%.

Experiments [4] show that for large currents, and hence larger amplitudes, the frequency/current relationship significantly deviates from linearity. In order to account for this, Eq. (2) was solved numerically using the projection method where one renormalizes the magnetization after each time step in order to preserve the local conservation of $\vec{M}$ [see [13]]. The steady states of this parametrically forced/damped system are attractors. The initial condition $m(\rho, 0) = a\phi^{(0)}(\rho)$ was evolved in time over a large domain ($0 \leq \rho \leq 100$) until the solution relaxed to a steady state. The mode frequency was numerically recovered from the phase of the precessing transverse component as $\hat{\omega} = \frac{d}{dt} \arg[m(0,t)], \, t \to \infty$.

Typical modes, their frequencies, and currents are shown in Fig. 2. The transverse mode envelope $\pm m = \pm(m_x^2 + m_y^2)^{1/2}$ and the y component of magnetization m_y show
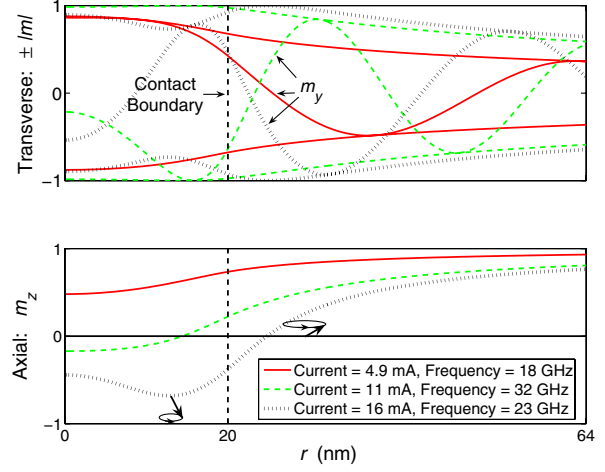

FIG. 2 (color online). Spatial dependence of fully nonlinear modes with excitation current and frequency. Top: transverse envelopes $\pm|m| = \pm\sqrt{m_x^2 + m_y^2}$ and associated spin waves m_y. Bottom: axial components m_z. For $j \geq j_{max}$, the transverse mode magnitude is no longer monotonically decreasing since the axial component of magnetization is negative ($m_z < 0$) in the point contact. Frequency and current values for each mode are shown as circles in Fig. 3.

slow decay, which means that spin waves are continually radiating away from the point contact, and hence energy from the contact region is lost into the surrounding medium.

The plot of frequency versus current in Fig. 3 shows a comparison between numerical simulation of (2), perturbation theory (5), and experiment [4]. For current excita-
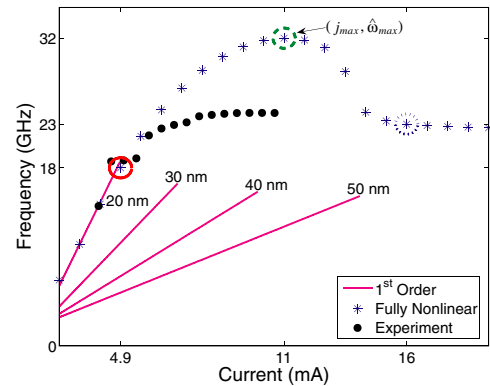

FIG. 3 (color online). Precession frequency as a function of current with comparison between fully nonlinear modes [direct numerical simulation of Eq. (2)], the perturbation result (5), and experiments conducted using $r_* = 20$ nm point contacts [4]. Large circles represent the frequency and current of modes plotted in Fig. 2. The straight lines were generated by perturbation theory [Eq. (5)] for the contact radii denoted. Note the excellent agreement between numerical simulation, perturbation theory, and experiment for small currents. The parameters have nominal values except $\epsilon = 0.8$.
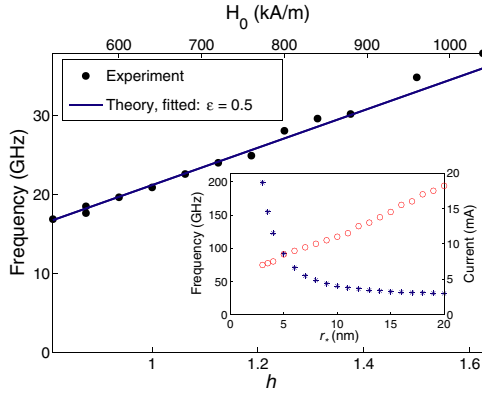
FIG. 4 (color online).   Frequency as a function of applied field h. Comparison between fully nonlinear modes [direct numerical simulation of Eq. (2)] and experiments [4]. Parameters are $I = 10$ mA and fitted $\epsilon = 0.5$. Inset: maximum frequency ($*$) and current ($\bigcirc$) vs contact radius.

tions larger than j_{max}, the solitary-wave mode structure becomes highly nonlinear (compare with Fig. 2). There is a maximum frequency and corresponding current for a given physical system (j_{max}, $\hat{\omega}_{max}$). As the dashed mode in Fig. 2 shows, frequency saturation corresponds to magnetization precession along the equator near the center of the point contact ($m_z \approx 0$). For currents less than j_{max}, the transverse mode magnitude has a monotonically decreasing dependence on r. For larger currents, the mode is not monotonic and develops interesting structure inside the point contact.

Figure 3 shows that, as the point contact size is increased, the slope of frequency versus current decreases because the slope depends on SMT torque (inversely proportional to r_*^2) and damping due to spin-wave generation [inversely proportional to r_* in the linear approximation [7]]. The comparison of the simulated results ($*$) with experiment is remarkable when the SMT efficiency is taken to be $\epsilon = 0.8$. As the experimental values of the frequency level out, full saturation is being reached. This is the first model to qualitatively capture this type of behavior.

Nominal values for ϵ are on the order of 0.25 for most ferromagnetic metals [14]. The fact that $\epsilon > 0.25$ is used to fit the experimental data suggests that further refinement of the model is desirable.

The dependence of frequency on applied magnetic field H_0 is depicted in Fig. 4. With the fitted SMT efficiency parameter, the theory compares well with experiment. The mode structure is highly nonlinear because the transverse amplitude is $|m(0, t)| \approx 0.98$, which precludes the use of Eq. (5). However, a full numerical solution is required for only one particular value of h. Since $d\hat{\omega}/dh \approx$ const for $\alpha \ll 1$, once the parameters α, j, and ρ_* are chosen, the y-intercept for the approximate linear relationship between $\hat{\omega}$ and h is fixed. The slope of the line does not change. The theory predicts the slope very accurately. In Fig. 4 inset, much higher frequencies are predicted by shrinking the size of the point contact. Using the method stated above, we predict that frequencies in the 0.2 THz range are attainable for a point contact with a radius of 3 nm. We find that as the point contact is made smaller, the current decreases linearly for the same reasons stated earlier in regard to the $\hat{\omega}(j)$ slope, while the frequency increases in proportion to $1/r_*^2$ due to exchange-mode spin-wave dispersion.

In summary, a model of magnetic excitations in point contact structures that includes nonlinearities due to both exchange and dipole coupling is introduced. Spatially dependent steady-state modes are calculated. This represents a large step forward in the explanation of the phenomena observed in recent experiments.

*Electronic address: hoefer@colorado.edu
[1] J. C. Slonczewski, J. Magn. Magn. Mater. **159**, L1 (1996).
[2] M. Tsoi *et al.*, Phys. Rev. Lett. **80**, 4281 (1998).
[3] S. I. Kiselev *et al.*, Nature (London) **425**, 380 (2003).
[4] W. H. Rippard *et al.*, Phys. Rev. Lett. **92**, 027201 (2004).
[5] G. Bertotti *et al.*, Phys. Rev. Lett. **94**, 127206 (2005); S. M. Rezende, F. M. de Aguiar, and A. Azevedo, Phys. Rev. Lett. **94**, 037202 (2005); A. N. Slavin and P. Kabos, IEEE Trans. Magn. **41**, 1264 (2005).
[6] L. Berger, Phys. Rev. B **54**, 9353 (1996).
[7] J. C. Slonczewski, J. Magn. Magn. Mater. **195**, L261 (1999).
[8] W. H. Rippard *et al.*, Phys. Rev. Lett. **95**, 067203 (2005).
[9] W. H. Rippard *et al.*, Phys. Rev. B **70**, 100406(R) (2004).
[10] L. D. Landau and E. M. Lifshitz, *Statistical Physics Part 2* (Butterworth-Heinemann, London, 1980), 3rd ed.
[11] Y. B. Bazaliy, B. A. Jones, and S.-C. Zhang, Phys. Rev. B **57**, R3213 (1998); M. D. Stiles and A. Zangwill, Phys. Rev. B **66**, 014407 (2002).
[12] J. D. Cole, *Perturbation Methods in Applied Mathematics* (Blaisdell, Waltham, 1968).
[13] W. E. Wang and X.-P. Wang, SIAM J. Numer. Anal. **38**, 1647 (2000).
[14] M. R. Pufall, W. H. Rippard, and T. J. Silva, Appl. Phys. Lett. **83**, 323 (2003).